



ACADEMIC  
PRESS

Available online at [www.sciencedirect.com](http://www.sciencedirect.com)

SCIENCE @ DIRECT®

Journal of Solid State Chemistry 174 (2003) 175–181

JOURNAL OF  
SOLID STATE  
CHEMISTRY

<http://elsevier.com/locate/jssc>

# Structural disorder along the lithium diffusion pathway in cubically stabilized lithium manganese spinel

## II. Molecular dynamics calculation

Kenji Tateishi,<sup>a</sup> Douglas du Boulay,<sup>a</sup> Nobuo Ishizawa,<sup>a,\*</sup> and Katsuyuki Kawamura<sup>b</sup>

<sup>a</sup> *Materials and Structures Laboratory, Tokyo Institute of Technology, 4259 Nagatsuta, Midori Yokohama 226-8503, Japan*

<sup>b</sup> *Department of Earth and Planetary Sciences, Tokyo Institute of Technology, 2-12-1 Oookayama, Meguro-ku, Tokyo 156-8552, Japan*

Received 25 July 2002; received in revised form 7 February 2003; accepted 9 April 2003

### Abstract

Molecular dynamics (MD) simulations were carried out to investigate the local structural disorder in  $\text{LiMn}_2\text{O}_4$  spinel. Small but significant shifts of lithium and oxygen atom positions from the high symmetry sites of the  $Fd\bar{3}m$  lattice were observed. The lithium atoms are displaced approximately  $0.16 \text{ \AA}$  away from  $8a$  site of the  $Fd\bar{3}m$  lattice and are shifted along the diffusion pathway towards the face midpoints of the coordinating  $\text{LiO}_4$  tetrahedra. A diffuse population of Li atoms was also detected centered about  $0.38 \text{ \AA}$  away from the  $16c$  octahedral vacancy, suggesting a portion of the Li atoms are free from their tetrahedral cages at room temperature. The tetrahedrally coordinated O atoms are displaced by as much as  $0.12 \text{ \AA}$  when bonded to one Li and three Mn atoms in identical oxidation states. On the other hand, if the coordinating Mn atoms are in mixed oxidation states, much larger O atom shifts of  $0.22 \text{ \AA}$  are observed. Structural features obtained in this MD simulation, especially the off-center displacements of Li and O atoms, are in accord with the electron density distribution study of cubically stabilized Mg-doped  $\text{LiMn}_2\text{O}_4$  spinel reported in Part I. © 2003 Elsevier Science (USA). All rights reserved.

**Keywords:** Molecular dynamics simulations;  $\text{LiMn}_2\text{O}_4$ ; Lithium manganese spinel; Structural disorder; Lithium diffusion pathway

### 1. Introduction

It is often the case for solid solution compounds that the underlying parent structure accommodates local structural modifications by the solute atoms. This has been well studied for the fluorite-related compounds like cubically stabilized zirconia [1]. The lithium manganese spinel crystals can also be stabilized in an archetypal cubic form by partial substitution of Mn with other metal atoms such as Mg or Co [2–5]. The cubically stabilized lithium manganese oxides are potential candidates for the positive electrode material of rechargeable Li ion batteries. The local structural disorder caused by the statistical distribution of different atoms at the same crystallographic site is not well known though it is deeply related to the mechanism of Li diffusion. In cubically stabilized lithium manganese spinel the existence of two different Mn oxidation states,

III and IV, further complicates the structural disorder [6–10].

The X-ray diffraction study reported in Part I revealed the following evidence of structural disorder in the Mg-stabilized cubic lithium manganese oxide,  $\text{Li}(\text{Mg}_{1/6}\text{Mn}_{11/6})\text{O}_4$ : (1) the structure is essentially of spinel-type with a faint diffuse scattering; (2) the electron density distribution at the  $8a$  sites with four lobes extended along  $\langle 111 \rangle$  suggests possible static or dynamic disorder associated with the Li atoms at those sites; (3) the accumulation of residual electrons  $0.35 \text{ \AA}$  away from the  $16c$  octahedral interstices suggests the existence of a minor population of Li atoms at those sites; and (4) the O atoms exhibit substantial charge density redistribution, evidence of static or dynamic disorder associated with their ideal positions.

Since the electron density distribution obtained by X-ray diffraction is essentially a time and spatially averaged, static image of the unit cell, any interpretation of the positional disorder features contained therein is inherently ambiguous unless it can be verified by some

\*Corresponding author. Fax: +81-45-924-5360.

E-mail address: [nishizaw@n.cc.titech.ac.jp](mailto:nishizaw@n.cc.titech.ac.jp) (N. Ishizawa).

complementary method. The present study of the molecular dynamics (MD) in cubically stabilized lithium manganese spinel by means of computer simulation, is ideally suited to provide this complementary information.

## 2. Experimental

MD calculations were undertaken using the MXDORTO program [11]. For simplification, the presence of Mg atoms in lithium manganese spinel  $\text{Li}(\text{Mg}_{1/6}\text{Mn}_{11/6})\text{O}_4$  was neglected and the stoichiometric composition  $\text{LiMn}_2\text{O}_4$  was assumed. An extended cubic MD cell with a dimension of  $33.004 \text{ \AA}$ , containing 512 Li, 512 Mn(III), 512 Mn(IV) and 2048 O independent atoms was modeled. The Mn(III) and Mn(IV) atoms were randomly assigned to the  $Fd\bar{3}m$   $16d$  sites as initial configurations. Periodic boundary conditions were applied in all directions. All atoms in the MD cell were allowed to move in any direction resulting in  $P1$  symmetry for the MD cell. Atomic motions were calculated using the Verlet algorithm [12] with the electrostatic interactions calculated using the Ewald split summation technique [13]. The pair potential used in this study was of Gilbert–Ida-type [14]

$$U(r_{ij}) = Z_i Z_j e^2 / r_{ij} + f_0 (b_i + b_j) \exp[(a_i + a_j - r_{ij}) / (b_i + b_j)]. \quad (1)$$

Here  $Z_i$  is the effective atomic charge,  $e$  is the elementary electric charge,  $r_{ij}$  is the interatomic distance,  $f_0$  is a constant, and  $a_i$  and  $b_i$  represent the size and stiffness parameters, respectively. The same potential parameters as those derived by Suzuki et al. [7], were used in this study and listed in Table 1. The short range potential and the real space component of the Ewald summation were truncated at 7.5 and 15  $\text{Å}$ , respectively. Calculations were performed mainly at 300 K with supplementary ones at various temperatures below 600 K, by controlling the atomic velocities. The calculations were performed using an NTP ensemble at 2 fs intervals for 60,000 steps, 120 ps in total. The MD calculations were repeated four times with different Mn(III) and Mn(IV) starting configurations to confirm that the general results were independent of those assignments. An additional MD calculation was per-

Table 1  
Potential parameters

Atoms	$Z$	$a$ ( $\text{Å}$ )	$b$ ( $\text{Å}$ )
Li	+1.0	1.043	0.080
Mn(III)	+1.4	1.038	0.070
Mn(IV)	+2.4	0.958	0.070
O	-1.2	1.503	0.075

formed assuming a unique oxidation state for all Mn atoms for comparison with the aliovalent model.

## 3. Results and discussion

The calculated unit-cell parameters and atomic coordinates at 300 K are listed in Table 2. The calculated unit-cell dimension  $8.250 \text{ Å}$  is in good agreement with  $8.2468 \text{ Å}$ , the reported value for  $\text{LiMn}_2\text{O}_4$  [15]. The positional parameters averaged over the whole MD cell are also in good agreement with those obtained by the neutron diffraction for  $\text{LiMn}_2\text{O}_4$  [15] and Mg-stabilized cubic  $\text{Li}(\text{Mg}_{1/6}\text{Mn}_{11/6})\text{O}_4$  in Part I.

A measure of the distribution of interatomic distances between selected atom pairs is provided by the pair correlation function, expressed as

$$g_{ij}(r) = \frac{V}{N_i N_j} \sum_{i=1}^{N_i} \frac{n_{ij}}{4\pi r^2 \Delta r}, \quad (2)$$

where  $V$  is the volume of a unit cell and  $N_i$  and  $N_j$  are the number of atoms  $i$  and  $j$ , respectively,  $n_{ij}$  is the number of atoms  $j$  in the spherical shell between radius  $r - \Delta r/2$  and radius  $r + \Delta r/2$  centered on the atom  $i$ . The pair correlation functions for Mn(III)–O and Mn(IV)–O at 300 K are shown in Fig. 1. Each curve has two peaks corresponding to the first and second nearest-neighbor shells. Mn(IV) is surrounded by six O atoms at an average distance of  $1.82 \text{ Å}$  while the averaged Mn(III)–O interatomic distance is  $2.00 \text{ Å}$ . The difference between the mean Mn(III)–O and Mn(IV)–O distances for the second shell is less significant owing to their dispersed profiles. The Mn(Mg)–O interatomic distance determined from X-ray diffraction in  $\text{Li}(\text{Mg}_{1/6}\text{Mn}_{11/6})\text{O}_4$  in Part I was  $1.969(1) \text{ Å}$ , which is closer to the mean Mn(III)–O distance in the present study.

A notable feature of the present simulation results is that Li atoms have reduced populations at the ideal  $8a$  sites of the spinel structure. The final atomic positions of all Li atoms having the same tetrahedral orientation

Table 2  
Calculated lattice parameter and atomic coordinates of  $\text{LiMn}_2\text{O}_4$

	Lattice parameters ( $\text{Å}$ )	
	MD	Expt [15]
	8.250	8.2468
Atoms	Atomic coordinates	
	$x(=y=z)$ , MD	$x(=y=z)$ , Expt [15]
Li	0.12496	0.125
$\text{Mn}^{3+}$	0.50056	0.5
$\text{Mn}^{4+}$	0.49953	0.5
O	0.26303	0.2625 (1)

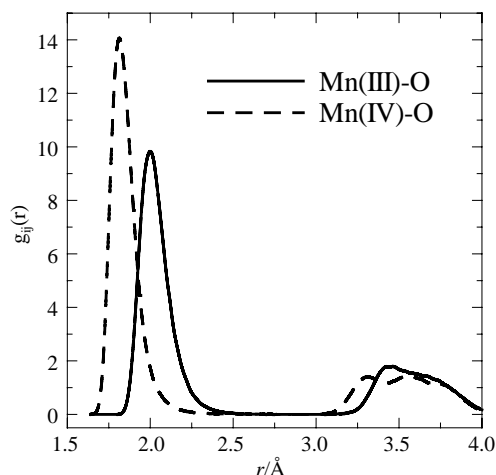


Fig. 1. Pair correlation functions of Mn(III)-O (solid line) and Mn(IV)-O (broken line) at 300 K.

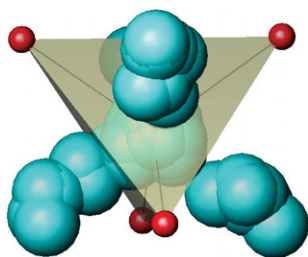


Fig. 2. Distribution of Li atoms in  $\text{LiMn}_2\text{O}_4$  spinel structure. Some Li atoms have hopped out from the coordination tetrahedron of O atoms depicted by small sphere.

relationship are superimposed and shown in Fig. 2. It can be seen that some Li atoms are displaced along  $\langle 111 \rangle$  to such an extent that they breach their ideal  $\text{LiO}_4$  tetrahedral bonding constraints. This direction lies along the line connecting the  $8a$  sites with the octahedral interstices at  $16c$ .

The frequency distribution of the radial displacements of Li from the ideal  $8a$  site, shown in Fig. 3, was obtained numerically from the positions of the 512 Li atoms observed over 10,000 steps for the period  $100 < t \leq 120$  ps at 2 fs intervals. Because this figure is not a radial probability density function, which would be strongly maximized at  $r = 0$ , the median radial Li displacement as characterized by the large peak around  $r = 0.16$  Å from  $8a$  can only be interpreted as a measure of spread of Li atoms about that site. However, Fig. 3 does highlight the existence of a subsidiary diffuse population peak around  $1.4$  Å from  $8a$  of the  $Fd\bar{3}m$  lattice as well as the fact that no Li atoms diffused further than  $2.4$  Å from  $8a$ . The second peak located  $1.4$  Å from  $8a$  corresponds to  $0.38$  Å away from the  $16c$  site.

The probability density functions (pdf's) of selected Li atoms for the same period are displayed in Fig. 4 in

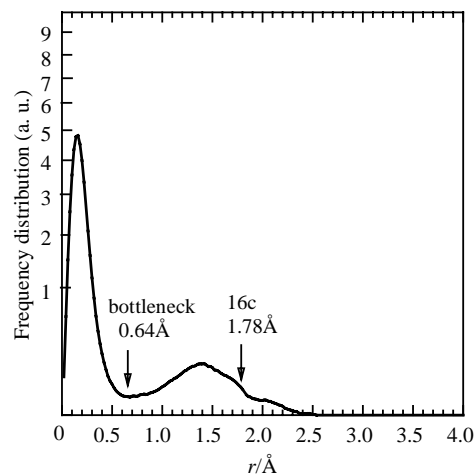


Fig. 3. Frequency distribution of the displacements of 512 Li atoms as a function of distance  $r$  from  $8a$  of the  $Fd\bar{3}m$  lattice.

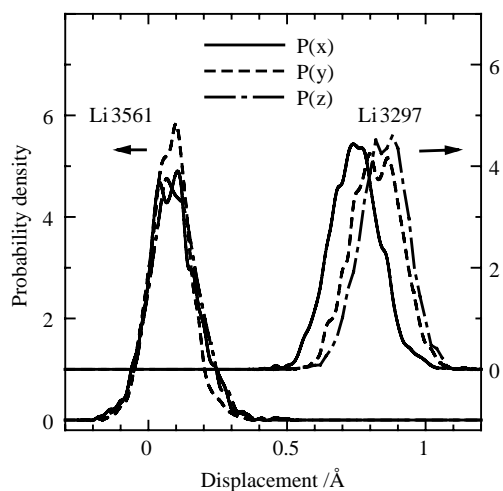


Fig. 4. Probability density functions of Li3561 in a tetrahedral cage and of Li3297 out of the cage. The displacements  $\Delta x$ ,  $\Delta y$  and  $\Delta z$  along the principal axes are referred to their positions at  $8a$  of the  $Fd\bar{3}m$  lattice.

order to reveal characteristic displacements of individual Li atoms contributing to the total averaged probability density. It is noted that each Li atom exhibits a relatively sharp Gaussian-type pdf which is not centered around the ideal  $8a$  site. The Li3561 atom which is vibrating about an equilibrium position  $\Delta x \approx \Delta y \approx \Delta z \approx 0.09$  Å from  $8a$  has a symmetrical Gaussian-type profile with the full-width at half-maximum (FWHM) of  $0.17$  Å, while the Li3297 atom which vibrates about an equilibrium position  $\Delta x \approx \Delta y \approx 0.85$  Å and  $\Delta z \approx 0.75$  Å from  $8a$  of the  $Fd\bar{3}m$  lattice has a slightly broader profile with FWHM of  $0.22$  Å indicating that Li3297 is vibrating in a shallower potential well than Li3561. The distance of the former from  $8a$  of the  $Fd\bar{3}m$  lattice is  $0.16$  Å, which corresponds closely to the first peak in Fig. 3. The pdf's of other Li atoms are broadly similar to Li3561 or Li3297 depending on their locations, i.e.,

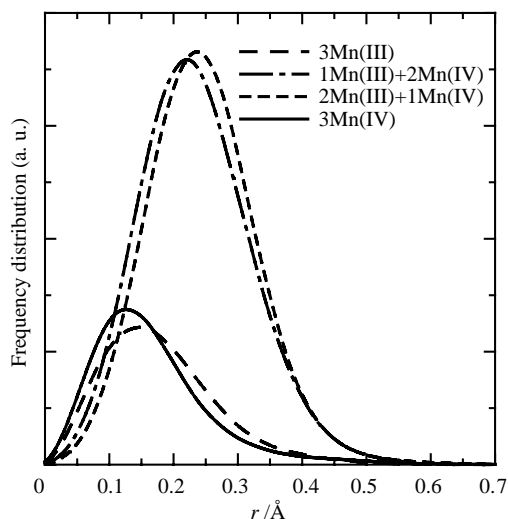


Fig. 5. Frequency distribution of the displacements of O atoms in four different coordination tetrahedra composed of one Li and three Mn with the oxidation states of III and IV, as a function of distance  $r$  from the ideal  $32e$  site in  $Fd\bar{3}m$ . The distributions are weighted by the number of O atoms in each group.

within the tetrahedral cage or not. The pdf's in Fig. 4 strongly support a structural model in which the Li atoms are statically disordered and vibrating harmonically rather than vibrating anharmonically about the  $8a$  site.

It is interesting to compare the Li atom distributions obtained by the MD calculation with the residual electron densities observed in the difference Fourier map by X-ray diffraction on the stoichiometric compound  $\text{LiMg}_{1/6}\text{Mn}_{11/6}\text{O}_4$  (Fig. 5 in Part I). In the X-ray diffraction experiment only the time and spatial average of the Li atom positions are highlighted. So even though the most populated Li region in the difference Fourier map is located at the  $8a$  site, the aspherical tetrahedral distribution projecting along  $\langle 111 \rangle$  is completely consistent with a spatial average of tetrahedrally displaced, off-centered Li atoms with a pdf maximized around  $0.16 \text{ \AA}$  from the  $8a$  site as characterized by Li3561 atom in Fig. 4. The subsidiary Li populated region  $1.0\text{--}1.7 \text{ \AA}$  from  $8a$  of the  $Fd\bar{3}m$  lattice along the  $8a\text{--}16c$  tie-line in Fig. 5 of Part I is consistent with the superposition of a distribution of sites analogous to Li3297 in Fig. 4. The authors consider this agreement to be strong evidence in favor of the split Mn valence model and the superiority of a split-site harmonic vibration model over the anharmonic vibrational model. The zero values beyond  $2.4 \text{ \AA}$  in Fig. 3 indicate that the self-diffusion of Li atoms did not progress further than that point.

In  $\text{LiMn}_2\text{O}_4$  spinel the O atoms are tetrahedrally coordinated by one Li and three Mn atoms. Consequently, four possible  $[\text{OLiM}_3]^{n+}$  tetrahedral configurations can arise depending on the Mn oxidation state ( $M = \text{Mn(III)}$  or  $\text{Mn(IV)}$ ,  $n = +8, +9, +10$  or  $+11$ ).

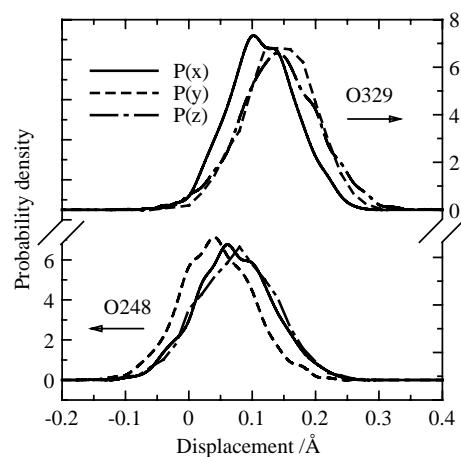


Fig. 6. Probability density functions of O248 surrounded by three Mn(IV) and one Li, and O329 surrounded by one Mn(III), two Mn(IV) and one Li. The displacements  $\Delta x$ ,  $\Delta y$  and  $\Delta z$  along the principal axes are referred to their positions at the  $32e$  site of the  $Fd\bar{3}m$  lattice.

This is the most probable origin of the observed O atom displacements, which occur in order to balance the electrostatic forces within the tetrahedra.

The displacements of O atoms in four different coordination tetrahedra can be seen from the weighted radial displacement frequency distributions of the O atoms in Fig. 5, where the weight is given by the number of sites with the same coordination. The distribution was calculated in the same manner as for Li with sums accumulated over the time period from  $100 < t \leq 120 \text{ ps}$  at  $2 \text{ fs}$  intervals. If one of the three coordinating Mn atoms has an oxidation state different from the other two, the O atom may be displaced by up to  $0.22 \text{ \AA}$ . The displacements are much smaller,  $0.10\text{--}0.13 \text{ \AA}$ , when three Mn ions have identical oxidation states.

The pdf's of O248 and O329 are calculated in the same way as those of the Li atoms and shown in Fig. 6. The O248 atom is surrounded by three Mn(IV) and one Li, while O329 is surrounded by one Mn(III), two Mn(IV) and one Li. The figure indicates that the O atoms are vibrating almost harmonically about their respective mean displaced positions.

Since the  $\text{OLiMn}_3$  and  $\text{LiO}_4$  tetrahedra interpenetrate, the displacement of O atoms is directly linked to the deformation of the  $\text{LiO}_4$  tetrahedra. When an O atom is displaced so as to enlarge a face of the  $\text{LiO}_4$  tetrahedron, it aids the Li diffusion through the opening. It is quite conceivable that changes in the oxidation states of the Mn ions as a function of time, under the influence of an applied potential for instance, could further complicate the  $\text{LiO}_4$  tetrahedral deformation dynamics. A dynamic change of the oxygen atom positions should occur in association with the electron hopping between Mn cations, which in turn may activate the diffusion of nearby Li atoms.

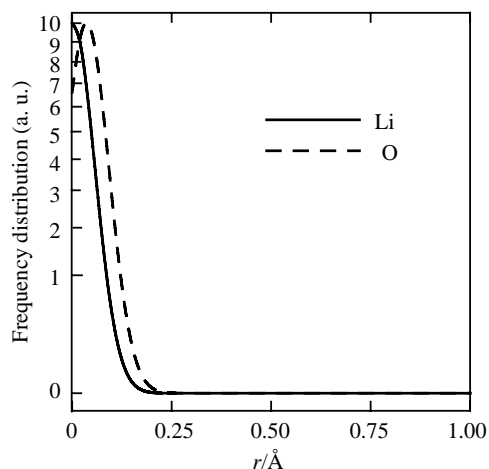


Fig. 7. Frequency distribution of the displacements of Li and O assuming a single oxidation state of 3.5 for all Mn from respective ideal positions.

To confirm that these effects arise from the existence of two distinct Mn oxidation states, a counter simulation was performed in which a single, fixed oxidation state of +3.5 was assigned to all Mn atoms. Potential parameters for Mn were the mean of those for Mn(III) and Mn(IV). The radial distribution functions for Li and O atoms using this model are shown in Fig. 7. In such a resonant state, the displacements of oxygen atoms was very small in comparison to the MD calculations assuming the coexistence of distinct Mn(III) and Mn(IV). The Li atoms did not shift significantly from the  $8a$  site. Because this result is discordant with the diffraction results as shown in Fig. 5 of Part I, the model appears inappropriate compared with that assuming the presence of distinct Mn(III) and Mn(IV) electronic states in the  $\text{LiMn}_2\text{O}_4$  structure.

The mean square displacements (msd's) of the constituent atoms as a function of time  $t$  can be calculated from their coordinates  $r(t)$  with respect to the original positions at  $t = t_0$ :

$$\text{msd}(t) = \overline{|r(t) - r(t_0)|^2}, \quad (3)$$

where the overline upon the right equation represents the average over all the atoms of the same species in the MD cell. The msd of Li at 300 K is shown in Fig. 8, where  $t_0$  was taken as 0. The value increases from the commencement of MD calculation up to 40 ps as initial strains are relaxed and then becomes constant at about  $0.27 \text{ \AA}^2$ . The msd of Li at various temperatures are shown in Fig. 9. They also become constant after a short relaxation time of approximately 40 ps. According to the random walk theory, the msd of a migrating atom in a solid increases linearly with time [16]. The time-independent nature of the msd of Li after relaxation therefore suggests that Li does not diffuse appreciably at temperatures below around 400 K after relaxation.

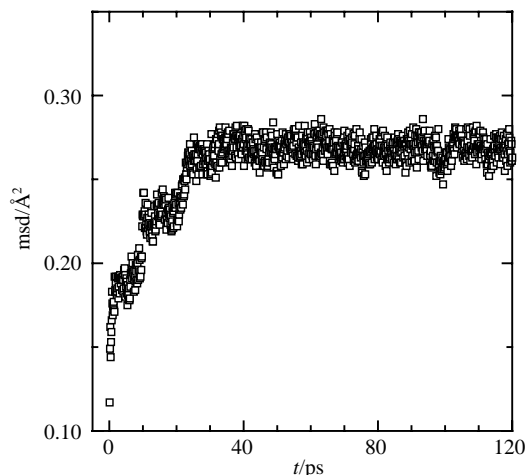


Fig. 8. Mean square displacements of Li in  $\text{LiMn}_2\text{O}_4$  at 300 K as a function of time.

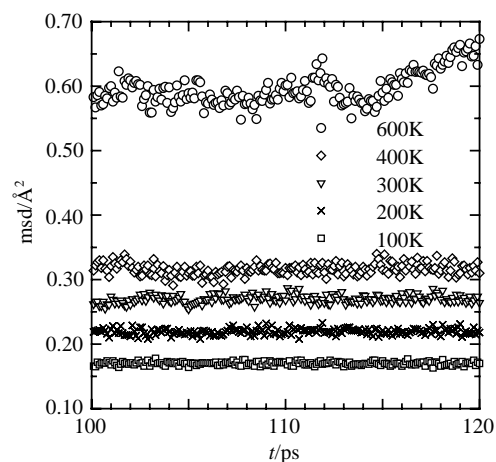


Fig. 9. Mean square displacements of Li in  $\text{LiMn}_2\text{O}_4$  at various temperatures as a function of time after relaxation.

The Li msd of  $0.27 \text{ \AA}^2$  was far larger than the displacement parameter of  $0.012 \text{ \AA}^2$  obtained from the X-ray diffraction study in Part I. This stems from the fact that the msd calculated from Eq. (3) includes the relaxation phase to distribute atoms statistically among various stable positions near the ideal positions at the early stage of the MD simulation. To estimate these initial offsets,  $\text{msd}_{\text{stat}}$  was calculated as

$$\text{msd}_{\text{stat}}(t) = \overline{|\langle r(t) \rangle_{\text{stat}} - r(t_0)|^2}. \quad (4)$$

Here the time-average surrounded by the angle brackets with subscript stat was taken over the time interval  $100 < t < 120$  ps for all atoms in the MD cell. The  $\text{msd}_{\text{therm}}$ , which mainly arises from the thermal fluctuation of atoms after relaxation, was then calculated as

$$\text{msd}_{\text{therm}}(t) = \overline{|\langle r(t) - \langle r(t) \rangle_{\text{stat}}|^2}. \quad (5)$$

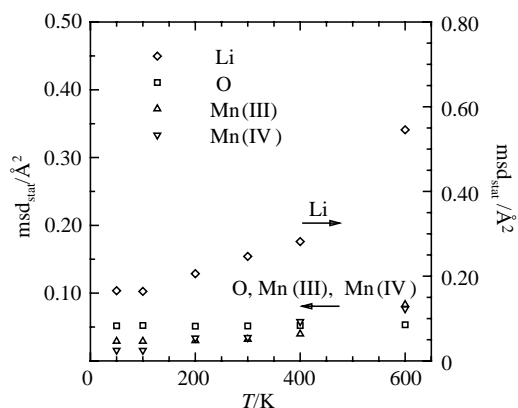


Fig. 10. Changes of static components of the mean square displacement in  $\text{LiMn}_2\text{O}_4$  with temperature.

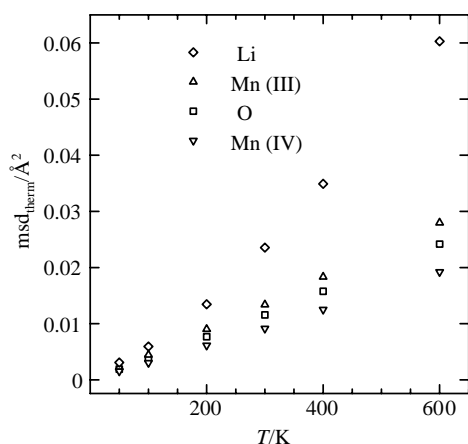


Fig. 11. Changes of thermal components of the mean square displacement in  $\text{LiMn}_2\text{O}_4$  with temperature.

Here the time-average was taken over  $100 < t < 120$  ps. Temperature dependence of  $\text{msd}_{\text{stat}}$  and  $\text{msd}_{\text{therm}}$  are shown in Figs. 10 and 11, respectively. These figures indicate that  $\text{msd}_{\text{stat}}$  is a major component of the overall  $\text{msd}$  values.

The  $\text{msd}_{\text{therm}}$  of Mn and O at 300 K in Fig. 11 have similar values to those obtained by X-ray diffraction in Part I, and are proportional to temperature. On the other hand, the increase of the Li  $\text{msd}_{\text{therm}}$  contains a higher order component. The accelerated increase of Li  $\text{msd}_{\text{stat}}$  in Fig. 10 is mainly attributed to large static displacements of the Li atoms, which hop out from the tetrahedral bounds. The number of these Li atoms stabilized at the positions outside the bottleneck point on the face of O tetrahedron is shown in Fig. 12. The number is constant below 125 K and increases monotonically above that temperature. The temperature dependency of  $\text{msd}_{\text{stat}}$  after excluding those Li atoms outside the tetrahedral enclosure is shown in Fig. 13. The Li  $\text{msd}_{\text{stat}}$  becomes smaller than the  $\text{msd}_{\text{stat}}$  of O and its dependence on temperature is less pronounced.

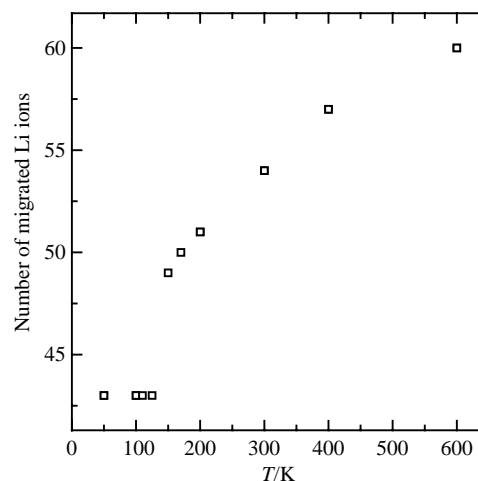


Fig. 12. Temperature dependence of the numbers of Li atoms which hop through the tetrahedral bottleneck point.

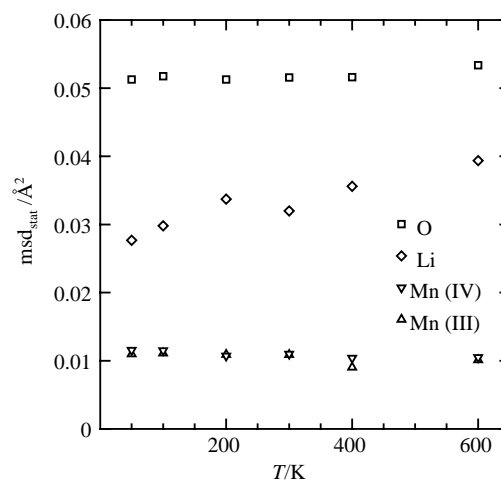


Fig. 13. Temperature dependence of the static components of the mean square displacement in  $\text{LiMn}_2\text{O}_4$  after excluding the atoms which hopped out from the coordinating polyhedra.

#### 4. Conclusion

MD simulations on cubic  $\text{LiMn}_2\text{O}_4$  at 300 K revealed small but significant shifts of lithium and oxygen atom positions from their ideal positions in the archetypal crystal structure with  $Fd\bar{3}m$  symmetry. Most lithium atoms appear to be statically displaced approximately  $0.16 \text{ \AA}$  away from  $8a$  of the  $Fd\bar{3}m$  lattice and the remainder are further statically distributed along the diffusion pathway connecting the  $8a$  tetrahedral site and the  $16c$  octahedral interstice. The tetrahedrally coordinated O atoms are displaced by as much as  $0.12 \text{ \AA}$  when bonded to one Li and three Mn atoms in identical oxidation states. On the other hand, if the coordinating Mn atoms are in mixed oxidation states then much larger O atom shifts of  $0.22 \text{ \AA}$  are observed.

The msd of Li increases with time during the earlier stages of the 300 K simulation up to the 40 ps mark due to structural relaxation where it stabilizes at  $0.27 \text{ \AA}^2$ , suggesting that further diffusion of Li no longer occurs. The MD simulations at various temperatures show that this tendency is retained up to approximately 400 K. The apparently large msd of Li stems from relatively large displacements from their ideal positions, which occur during the relaxation phase.

Structural features obtained in the present MD simulations, especially the off-center displacements of Li and O atoms, are in accord with the charge density study of cubically stabilized Mg-doped  $\text{LiMn}_2\text{O}_4$  spinel reported in Part I. The presence of many available positions for Li along the diffusion pathway may reduce the activation energy among local minima and facilitate the Li diffusion in the presence of chemical potential gradient.

### Acknowledgments

This study was supported by Grant-in-Aid for Scientific Research on Priority Areas (B) (No. 740) from The Ministry of Education, Science, Sports and Culture of Japan. DDB acknowledges JSPS fellowship P02148.

### References

- [1] N. Ishizawa, Y. Matsushima, M. Hayashi, M. Ueki, *Acta Crystallogr. B* 55 (5) (1999) 726–735.
- [2] R. Bittihn, R. Herr, D. Hoge, *J. Power Sources* 43 (1993) 223–231.
- [3] G. Pistoia, G. Wang, *Solid State Ionics* 66 (1993) 135–142.
- [4] G. Li, H. Ikuta, T. Uchida, M. Wakihara, *J. Electrochem. Soc.* 143 (1) (1996) 178–182.
- [5] N. Hayashi, H. Ikuta, M. Wakihara, *J. Electrochem. Soc.* 146 (4) (1999) 1351–1354.
- [6] Y. Shiraishi, I. Nakai, T. Tsubata, T. Himeda, F. Nishikawa, *J. Solid State Chem.* 133 (1997) 587–590.
- [7] K. Suzuki, Y. Oumi, S. Takami, M. Kubo, A. Miyamoto, M. Kikuchi, N. Yamazaki, M. Mita, *Jpn. J. Appl. Phys.* 39 (2000) 4318–4322.
- [8] J.E. McGrady, R. Stranger, *J. Am. Chem. Soc.* 119 (36) (1997) 8512–8522.
- [9] R. Stoyanova, M. Gorova, E. Zhecheva, *J. Phys. Chem. Solids* 61 (2000) 609–614.
- [10] J. Sugiyama, T. Hioki, S. Noda, M. Kontani, *J. Phys. Soc. Jpn.* 66 (4) (1997) 1187–1194.
- [11] K. Kawamura, MXDORTO, Japan Chemistry Program Exchange, #026.
- [12] L. Verlet, *Phys. Rev.* 159 (1967) 98–103.
- [13] P.P. Ewald, *Ann. Phys.* 64 (1921) 253–287.
- [14] Y. Ida, *Phys. Earth Planet. Interiors* 13 (1976) 97–104.
- [15] C. Fong, B.J. Kennedy, M.M. Elcombe, *Z. Kristallogr.* 209 (1994) 941–945.
- [16] P.G. Shewmon, *Diffusion in Solid*, McGraw-Hill Book Company, New York, NY, 1963, pp. 47–54.